# Stochastic Simulation of Inhomogeneous Metocean Fields. Part II: Synoptic Variability and Rare Events

Alexander V. Boukhanovsky[1], Harald E. Krogstad[2], Leonid J. Lopatoukhin[3], Valentin A. Rozhkov[3], Gerassimos A. Athanassoulis[4], and Christos N. Stephanakos[4]

[1] Institute for High Performance Computing and Information Systems, St. Petersburg, Russia
avb@fn.csa.ru, http://www.csa.ru
[2] Dept. Mathematical Sciences, NTNU, Trondheim, Norway
harald.krogstad@math.ntnu.no
[3] Oceanology Dept., State University, St. Petersburg, Russia
leonid@LL1587.spb.edu
[4] Technical University of Athens, Athens, Greeece,
{mathan,chstef}@central.ntua.gr

**Abstract.** The paper discusses stochastic models for the synoptic variability of metocean fields using spatio-temporal impulse representations combined with Markov walks of storms in space. The models are fitted to an extensive data set of ocean wave fields from the Barents Sea and verified by studying the fields duration and extreme value properties.

## 1 Introduction

Metocean fields, like atmospheric pressure, wind speed, ocean waves etc., have a complex spatial and temporal variability. Traditionally, the approach for statistical formalization of such phenomena has been based on a *multiscale* hypothesis proposed by Andrey S. Monin [17]. The hypothesis suggests modeling the total variability by means of a set of stochastic models for each temporal scale separately, and with the interdependence taken into account parametrically.

Stochastic simulations on the scale of annual and inter-annual variations were considered in the first part of this paper [9], but for metocean fields such as ocean waves, the synoptic variability has more interest, since its impact on the total variation and the extreme events is higher.

The synoptic variability corresponds to temporal scales from a few hours to some days. For atmospheric processes, the associated spatial scales are 2000–3000 km, as opposed to 500–700 km for the oceanic ones. The nature of the synoptic variability may be explained as a stochastic alternation between *storms* and *calms*, that is, cyclones and anticyclones in the atmosphere [1], and storms and calms for wind and wave fields [15].

P.M.A. Sloot et al. (Eds.): ICCS 2003, LNCS 2658, pp. 223–233, 2003.

There have been many papers devoted to the analysis and statistical description of the marginal [2,3,4,10,15,20,21] and even joint [7,22] synoptic variability of metocean processes in terms of stochastic series at fixed points in space. However, these methods become complicated if we consider the variability of the full spatio-temporal fields. Currently, there are at least two different approaches:

- *The Euler approach*, considering the joint variability of the field in a set of fixed points.
- *The Lagrange approach*, considering the motion of spatial structures in the fields.

The Euler approach adopts multivariate time series models $\zeta_k(t) = \zeta(\mathbf{r}_k, t)$ for description and simulation [19]. In the Lagrangian approach, the alternation of storm and calm periods may be described in terms of *spatio-temporal* random events, or *impulses* [13,15,20]. In general, it is difficult to say which approach is best. However, for the analysis of extreme events over the whole field, the Lagrange's approach may be more reliable because it is independent of choice of particular grid points. In the present paper, we describe a computationally efficient method for stochastic simulation of the synoptic variations of metocean fields based on the Lagrange approach, and fit the model to an extensive data set from the Barents Sea. The model is verified against the data for *T*-years field extremes.

## 2 The Data Set

The ocean wave field is described in terms of the directional wave spectrum and today, advanced numerical models, based on the numerical integration of the wave action equations, produce directional spectra in a fine grid, using the wind field as input. In this paper, the NCEP/NCAR reanalyzed wind fields 1971–99 [12] and the 4th generation wave model *WaveWatch-v1.18* [23] have been applied for a simulation of a long-term set of ocean wave fields for the Barents Sea region (Fig.1). The time step in the simulations is 6 hours, and wind and wave measurements from Barents Sea buoys were used for verification [16].

Instead of using the full ensemble of calculated spectra [15], we consider here only the most basic parameter, the significant wave height, $h(\mathbf{r},t)$, defined as four times the standard deviation of the surface height. The synoptic variability is summarized in the long-term distribution of $h(t)$ in fixed points, and Table 1 shows seasonal averages of the median $h_{0.5}$ and the r.m.s. value $\sigma_h$ of $h$, for three locations in the Barents Sea, as marked in Fig. 1.

**Table 1.** Average wave height distribution parameters

| Parameters of long-term wave heights distributions | | | | | | | | |
|---|---|---|---|---|---|---|---|---|
| Region | 1 | | 2 | | 3 | | Total area | |
| | $h_{0.5}$ [m] | $\sigma_h$ [m] | $h_{0.5}$ [m] | $\sigma_h$ [m] | $h_{0.5}$ [m] | $\sigma_h$ [m] | $h_{0.5}$ [m] | $\sigma_h$ [m] |
| Winter | 2.2 | 1.5 | 2.0 | 1.4 | 1.9 | 1.5 | 2.2 | 0.9 |
| Spring | 1.4 | 1.2 | 1.2 | 1.1 | 1.1 | 1.3 | 1.4 | 0.8 |
| Summer | 0.9 | 0.6 | 0.8 | 0.6 | 0.7 | 0.6 | 0.8 | 0.3 |
| Autumn | 1.6 | 1.1 | 1.6 | 1.2 | 1.5 | 1.2 | 1.6 | 0.7 |

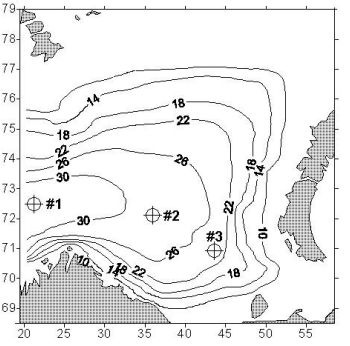


**Fig. 1.** Spatial distribution of 100-years maximal (0.1%) wave heights in the Barents Sea.

The data set is clearly spatially inhomogeneous [14] and the interval analysis, in accordance to [15], shows that the difference is significant, basically due to fetch limitations. The inhomogeneity of the wave field is even more clearly seen from a map of the spatial distribution of extreme events, *e.g.* waves encountered once 100 years (see Fig. 1). These results were obtained by the BOLIVAR method [15] applied to the same 28-years data. The highest waves are observed in the western part, and the intensity of the waves decreases towards SE.

## 3 The Spatial Parametrization of Storms

It is obvious from Table 1 and Fig. 1 that the wave fields are inhomogeneous in space and have the seasonal periodicity. We are going to describe these features in terms of spatial structures – *storms* and *calms*. For atmospheric phenomena this procedure is developed rather well, see, *e.g.* [1]. For ocean fields (such as ocean waves) it is possible to generalize Angelides' [2] definition of storms to the spatio-temporal domain,

$$\Omega(t) = \{\mathbf{r}: \quad h(\mathbf{r},t) \geq z\}, \tag{1}$$

where $z$ is the level of the storm and additional parameters are defined in Table 2. Note that $\{h^+, \mathbf{r}^+\}$ characterize the extreme and $\{\bar{h}, \mathbf{r}_0\}$ the general behavior of the storm in space.

Table 3 shows seasonally averaged storm statistics. The probability of storm occurrence is $P_{total}$, and the conditional probability for the numbers of storms is $P_N$. Thus, the level $z$ = 2m is exceeded in at least one point in 43.7% of the cases during winter. However, in only 1.4% of those cases the number of storms is greater than two.

The mean, r.m.s. and 95% quantiles for $h^+$, $\bar{h}$, and $L$ show that the parameters of the storms are strongly dependent on $z$ and have a clear annual variability. It is interesting to observe that the smallest storm diameter $L$ occurs in spring, and this may be caused by the seasonal variations of fetch related to the ice cover of the Barents Sea. The maximal ice cover (more that 60% of the sea area) is observed in March-April, and the minimal cover (10-15%) in September-October [8].

Geospatial vector statistics are displayed for vectors quantities [6,7,9]. These are the modulus and direction of the mean vector, $\{|\mathbf{m}|, \varphi_{\mathbf{m}}\}$, the principal axes and rotation

angle of the r.m.s. ellipse $\{\lambda_1, \lambda_2, \alpha\}$, and the coefficient of variation, $\rho = (\lambda_1^2 + \lambda_2^2)^{1/2} / |\mathbf{m}|$. It is seen that $\mathbf{r}^+$ is shifted from towards west $\mathbf{r}_0$, but less than about 50 km. The coefficient of variation $\rho$ is quite high, however.

**Table 2.** Characterizing parameters of the storms

| Description | Notation | Definition |
|---|---|---|
| Area | $S_\Omega(t)$ | $\int_{\Omega(t)} d\mathbf{r}$ |
| Equivalent diameter | $L(t)$ | $2\sqrt{S_\Omega(t)/\pi}$ |
| Averaging wave height | $\overline{h}(t)$ | $\int_{\Omega(t)} h(\mathbf{r},t)d\mathbf{r} \Big/ S_\Omega(t)$ |
| Geometric center ("center of gravity") | $\mathbf{r}_0(t)$ | $\int_\Omega h(\mathbf{r},t)\mathbf{r}d\mathbf{r} \Big/ \int_\Omega h(\mathbf{r},t)d\mathbf{r}$ |
| Maximum wave height | $h^+(t)$ | $\max_{\mathbf{r}\in\Omega(t)}\left[h(\mathbf{r},t)\right]$ |
| Location of the maximal wave height | $\mathbf{r}^+(t)$ | $\left\{\mathbf{r} : h(\mathbf{r},t) = h^+(t)\right\}$ |

Fig. 2 shows two examples of typical storms, six hours apart, with some of the above parameters marked on the map. The storm velocity, $\mathbf{W} = \partial\mathbf{r}_0 / \partial t$, and although the mean velocity of the storms is only 3.4-11.9 km/h, the variations may reach 50 km/h with large variability, as indicated by the relatively high values of both $\lambda_1$ and $\lambda_2$.

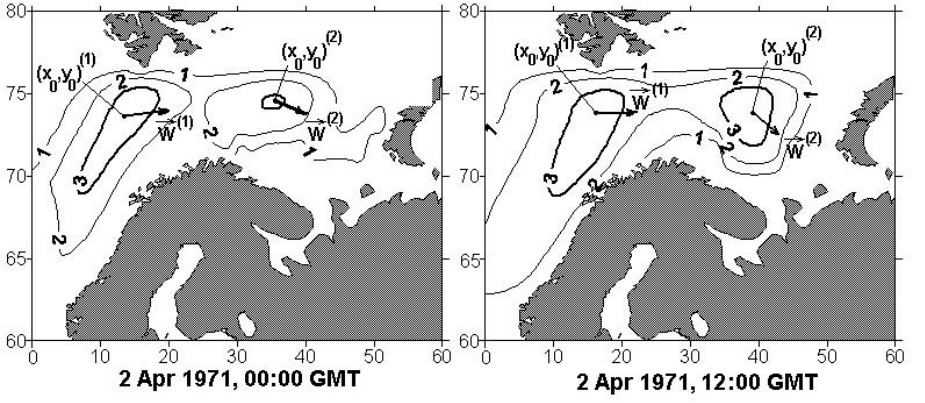


**Fig. 2.** Examples of storm movement in synoptic terms.

The analysis of Table 3 shows that, in general, only one storm occurs at a time, and the position of highest wave is not far from the storm's geometrical center, $\mathbf{r}_0$. Moreover, $\{h^+, L\}$ may be applied for defining the storm's spatio-temporal behavior.

**Table 3.** Seasonal estimates of parameters of the storms in the Barents sea. W – Winter, SP – Spring, SU – Summer, AU – Autumn. See text for further explanations.

| Parameter | | Level $z$ = 2.0 m | | | | Level $z$ = 4.0 m | | | |
|---|---|---|---|---|---|---|---|---|---|
| | | W | SP | SU | A | W | SP | SU | A |
| $P_{\text{total}}$ | | 43.7 | 30.6 | 23.2 | 47.3 | 20.5 | 6.2 | 1.0 | 12.5 |
| $P_N$ (%) | $N$=1 | 87.3 | 94.6 | 93.5 | 85.7 | 95.3 | 96.9 | 100 | 92.6 |
| | $N$=2 | 11.3 | 5.0 | 6.0 | 13.1 | 4.6 | 3.1 | – | 6.9 |
| | $N$≥3 | 1.4 | 0.4 | 0.5 | 1.2 | 0.1 | – | – | 0.5 |
| $h^+$ [m] | Mean | 2.4 | 2.4 | 2.3 | 2.4 | 4.5 | 4.4 | 4.3 | 4.4 |
| | r.m.s | 0.5 | 0.4 | 0.3 | 0.4 | 0.5 | 0.4 | 0.3 | 0.4 |
| | 95% | 4.0 | 3.7 | 3.2 | 3.6 | 6.2 | 5.3 | 5.1 | 5.8 |
| $\overline{h}$ [m] | Mean | 3.0 | 2.8 | 2.6 | 2.9 | 5.1 | 4.9 | 4.7 | 5.0 |
| | r.m.s | 1.1 | 0.8 | 0.6 | 0.9 | 1.1 | 0.8 | 0.6 | 0.9 |
| | 95% | 7.0 | 5.7 | 4.8 | 6.2 | 8.8 | 7.1 | 6.5 | 8.2 |
| $L$ [km] | Mean | 460 | 440 | 450 | 543 | 460 | 380 | 360 | 445 |
| | r.m.s. | 335 | 260 | 290 | 372 | 270 | 216 | 195 | 269 |
| | 95% | 1460 | 1200 | 1317 | 1592 | 1170 | 1000 | 910 | 1243 |
| $\mathbf{r}_0 - \mathbf{r}^+$ [km] | $\lvert\mathbf{m}\rvert$ | 45 | 49 | 18 | 47 | 31 | 35 | 16 | 13 |
| | $\varphi_{\mathbf{m}}$ | 276 | 258 | 314 | 284 | 255 | 238 | 354 | 286 |
| | $\lambda_1$ | 152 | 137 | 113 | 164 | 122 | 107 | 56 | 108 |
| | $\lambda_2$ | 96 | 78 | 81 | 120 | 84 | 65 | 46 | 82 |
| | $\alpha$ | 145 | 139 | 153 | 155 | 133 | 137 | 109 | 137 |
| | $\rho$ | 4.0 | 3.2 | 7.6 | 4.3 | 4.8 | 3.5 | 4.3 | 10.6 |
| Storm Center Velocity $\mathbf{W}$ [km/h] | $\lvert\mathbf{m}\rvert$ | 3.4 | 5.7 | 5.8 | 4.8 | 7.0 | 11.9 | 11.4 | 8.2 |
| | $\varphi_{\mathbf{m}}$ | 297 | 275 | 253 | 277 | 280 | 277 | 272 | 288 |
| | $\lambda_1$ | 28.0 | 20.3 | 21.1 | 29.4 | 24.1 | 19.6 | 20.1 | 22.3 |
| | $\lambda_2$ | 17.0 | 13.8 | 15.5 | 18.1 | 10.5 | 8.1 | 8.5 | 12.1 |
| | $\alpha$ | 180 | 150 | 153 | 180 | 137 | 130 | 136 | 134 |
| | $\rho$ | 9.7 | 4.33 | 4.5 | 7.11 | 3.7 | 1.8 | 1.9 | 3.09 |

## 4 A Stochastic Model for the Synoptic Variability

Traditional models are based on stochastic differential equations of the form

$$\frac{\partial h}{\partial t} + \mathbf{W} \cdot \nabla h = G(\mathbf{r}, t) , \tag{2}$$

where $G(\mathbf{r},t)$ is a source function. For wind waves, Eqn. (2) follows from the wave action equation [23] after integrating over the spectrum and linearizing the derivative term. If we expand the solution of Eqn. (2) using Galerkin techniques we obtain

$$h(\mathbf{r},t) = \sum\nolimits_k a_k(t) \Phi_k(\mathbf{r}, t \mid \Xi_k) , \tag{3}$$

where $\{\Phi_k\}$ are spatio-temporal basis functions, depending on a set of parameters $\Xi_k$, and $\{a_k\}$ the corresponding coefficients. The coefficients $\{a_k\}$ will be obtained as solutions of a system of algebraic equations after a suitable parametrization of $G$.

In contrast to this Eulerian approach, the Lagrange approach considered below writes the field as moving *spatio-temporal impulse structures*, and estimates the characteristics directly from the initial data set, without considering the source function.

### 4.1 Storm Motion

It is possible to model the temporal sequence of storm centres $\mathbf{r}_0(t)$ as a Markov chain with a finite number of spatial locations (regions). Fig. 3c shows a map with nine regions in the Barents Sea, and Table 4 estimates of the transition and limit probabilities of the Markov chain for the level $z$ = 2 (for all seasons). The additional ground state "C" (*calm*) signifies no storms.

**Table 4.** Transition and limit probabilities of the storm sequence. Here "+" is the probabilities below 1%, blank space – zero probabilities.

| State | Transition probabilities (%) | | | | | | | | | | Limit Prob. |
|---|---|---|---|---|---|---|---|---|---|---|---|
| | SW | S | SE | W | 0 | E | NW | N | NE | C | |
| SW | **11.7** | 17.2 | 2.2 | 15.6 | 20.6 | 2.2 | + | + | | 29.4 | 1.2 |
| S | 1.6 | **33.8** | 8.4 | 3.6 | 9.3 | 2.8 | + | + | + | 39.2 | 6.7 |
| SE | + | 9.8 | **27.3** | 3.3 | 4.3 | 5.5 | + | 1.6 | 2.7 | 44.7 | 3.3 |
| W | 3.5 | 8.1 | + | **31.3** | 23.2 | 1.4 | 1.2 | + | + | 28.6 | 5.4 |
| O | + | 11.2 | 3.9 | 5.8 | **44.2** | 10.1 | + | 2.4 | 1.8 | 19.9 | 9.3 |
| E | + | 4.9 | 10.2 | 2.8 | 8.6 | **25.3** | + | 1.4 | 7.2 | 38.8 | 2.9 |
| NW | 1.1 | 2.2 | 3.3 | 11.1 | 2.2 | | **14.4** | 16.7 | 1.1 | 47.8 | 0.6 |
| N | + | | 2.4 | 2.4 | 10.2 | 3.6 | 3.0 | **20.5** | 22.9 | 33.7 | 1.1 |
| NE | + | 2.1 | 1.4 | 2.8 | 4.5 | 3.1 | | 3.8 | **31.7** | 49.8 | 1.9 |
| C | + | 3.3 | 1.5 | 3.5 | 3.7 | 0.9 | 0.5 | 0.5 | 0.7 | **84.4** | 67.6 |

The diagonal elements dominate, showing that the storms tend to remain in the same region during one synoptic term. The limit probabilities show strong spatial inhomogeneity with the maximal occurrence of storms (9.3%) observed in the central region (O), and lowest in the NW, N, and SW regions. The Markov chain produces an alternating sequence of *storms* (of duration $\Im$) and *calms* (of duration $\Theta$).

### 4.2 Parametrization of Spatio-Temporal Impulses

Let us consider a storm $\{\mathbf{r}_0(t), h^+(t), S_\Omega(t)\}$, $t \in [t_0, t_0 + \Im]$. The size of the storm area $S_\Omega(t)$ may in fact be derived from a quantile diagram (Fig. 3a) of wave heights at a specific synoptic term *t*: $S_\Omega(t)$ is equal to the fraction of wave heights larger than $z$ times the total area of the region. It is also possible to apply a regression between $h^+$ and $S_\Omega(t)$. Some information about the *shape* of the storm area could be obtained from moments of inertia parameters $(\lambda_1, \lambda_2, \alpha)$, similar to those in Table 2.

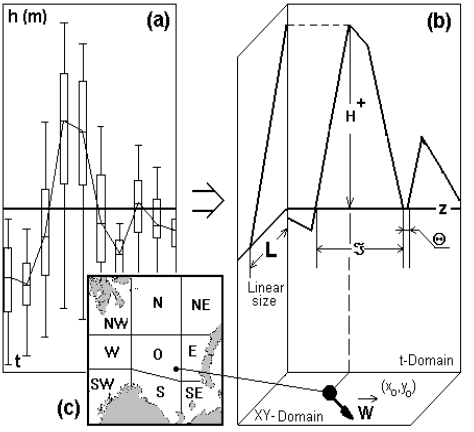


**Fig. 3.** The spatio-temporal parametrization of storm variability.

Our aim is to parametrize the storm impulses in terms of the overall maximum wave height $H^+$ and the associated storm area $S^+$. This parametrization, given in terms of a set of parameters $\{H^+, S^+, \Im, \Theta\}$ and the Markov process for $\mathbf{r}_0(t)$, generalizes the BOLIVAR approach [15,20] from time series to spatio-temporal fields. The data have shown that as the values $(H^+, \Im)$ as $(H^+, L^+)$ are highly dependent: (couple correlation are 0.7–0.9).

Since $H^+$ is an extreme value, the distribution, conditional on $\Im$, is approximately Gumbel,

$$F\left(H^+ \mid \Im\right) = \begin{cases} \exp\left[-\exp\left(-\left(H^+ - A(\Im)\right)/B(\Im)\right)\right], & H^+ \geq z, \\ 0, & H^+ < z, \end{cases} \tag{4}$$

and this has been validated in [20].

It now remains to specify a time function for $h^+(t)$ and a spatial field function $\Phi(\mathbf{r})$ as in Eqn. 3. It is shown in [15] that a piecewise linear function in time is sufficient, whereas for $\Phi(\mathbf{r})$ it is possible to use an elliptic cone (1st order), or a elliptic paraboloid (2nd order), see also Section 5 below.

### 4.3 Simulation Procedure

The simulation procedure is shown in Fig. 4. In first step is to estimate the parameters in Table 2 for each synoptic term *t*. The level *z* may depend on the season and obtained from models of the annual variability, as described in [9]. The second step is the spatio-temporal impulse parametrization of the time series $\{h^+(t), L(t)\}$, the parameters of Eqn. (4), and the parameters (transition and limit probabilities) of the Markov chain model for $\{\mathbf{r}_0(t)\}$.

The simulation starts with the Monte-Carlo simulation. Based on the realizations, the durations $\{\Im_k\}$ are found and the value of $H^+$ are simulated from Eqn. (4). The diameter $L^+$ is obtained regression on $H^+$, and finally, all synthesized parameters are substituted into Eqn. (3), thus generating a synthetic field for all points $(\mathbf{r}, t)$.

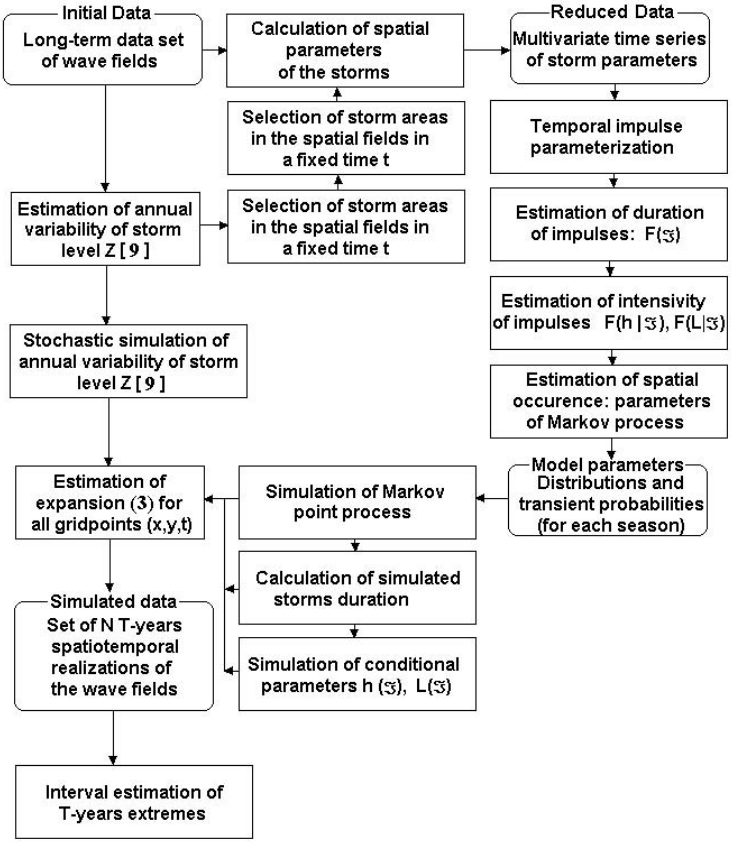


**Fig. 4.** Scheme of stochastic simulation procedure of synoptic variability

## 5 Verification and Extreme Value Analysis

There arise at least three questions for verification of the simulation procedure:

- Does the empirical storm duration statistics fit the Markov model statistics?
- Does the Lagrangian model described above reproduce the annual spatial extremes seen in the data?
- Does the Lagrangian model reproduce estimates of T-years extremes in the fixed points estimated by approaches like BOLIVAR or AMS [15]?

Figure 5 answers the first and second questions. Figure 5a shows the *quantile biplot* (Q-Q-plot) of simulated ($h^*$) and sample ($h$) values of annual maxima of significant wave height of over the whole sea. In Fig. 5b the same biplot is shown for simulated ($\vartheta^*$) and sample ($\vartheta$) values of storm durations. We observe good agreement between sample and simulated characteristics over the entire field. For answering the third question, the extremes for return period of 1, 10, and 100 years were calculated for the

points 1-3 in Fig. 1 by the AMS approach (with parametrical confidence intervals [15]) and by the Lagrangian stochastic simulation, see Table 5.

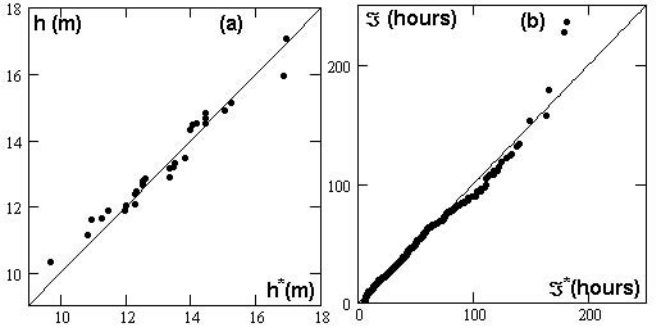


**Fig. 5.** Verification of the simulation model

All simulations were carried out for two types of the spatial impulse approximation $\Phi(\mathbf{r})$. The 1st order shape is an elliptic cone, and in this case the Lagrangian model underestimates the *T*-years extremes. By assuming the more reasonable form of an elliptical paraboloid for $\Phi(\mathbf{r})$, the values become in much better agreement with the AMS method.

**Table 5.** Sample and simulated values of *T*-year wave heights in Barents sea.

| Point | | 1 | | | 2 | | | 3 | | |
|---|---|---|---|---|---|---|---|---|---|---|
| T | | 1 | 10 | 100 | 1 | 10 | 100 | 1 | 10 | 100 |
| Sample estimates | Point data | 10.3 | 13.2 | 16.7 | 9.6 | 11.4 | 13.7 | 9.0 | 10.8 | 13.2 |
| | 90% | 9.3 | 11.9 | 15.0 | 8.6 | 10.3 | 12.3 | 8.1 | 9.7 | 11.9 |
| | conf. interval | 11.8 | 15.1 | 19.2 | 11.0 | 13.1 | 15.8 | 10.4 | 12.4 | 15.2 |
| Simulation | 1st order | 8.0 | 10.3 | 13.0 | 6.9 | 7.8 | 9.0 | 6.7 | 7.5 | 8.5 |
| | 2nd order | 9.8 | 12.2 | 15.1 | 9.2 | 11.6 | 14.5 | 8.4 | 10.6 | 13.4 |

The results of the model verification are satisfying and give confidence to use the Lagrangian model for analysis and numerical studies of the spatio-temporal variations of extreme synoptic events. Nevertheless, adaptation of the model to more complex sea basins is problematic and requires further development of the storm impulse approximations and the random walks model.

## 6 Conclusions

This paper has demonstrated that computational multivariate statistics of spatio-temporal fields may be used for describing the synoptic variability of metocean fields. The synoptic variability is modelled by a Lagrangian approach, which describes the storm motion by a spatial Markov random walk and the storm's extension and field properties as spatio-temporal impulses, characterized by a limited set of parameters.

Model properties not considered in the fitting have been used for verification, and the field extremes predicted by the model are shown to fit very well to estimates of extreme values obtained by other approaches.

**Acknowledgment.** This research has been partly founded by INTAS 99-0666 Project: "Estimation of extreme metocean events".

## References

1. Agee E.M. Trends in cyclone and anticyclone frequency and comparison with periods of warming and cooling over the Northern Hemisphere. J. Clim., 4, 1991, pp. 263–267.
2. Angelides D.C., Veneciano D., Shyam Sunder S. Random sea and reliability of offshore foundations. J. Eng. Mech. Div., 1981, vol. 107, #1, pp. 131–148.
3. Athanassoulis G.A., Vranas P.B., Soukissian T.H., 1992. A new model for long-term stochastic analysis and prediction. Journ. Ship Res., v 36, N1, pp. 1–16.
4. Athanassoulis G.A., Stephanakos Ch.N., 1995. A nonstationary stochastic model for lon g-term time series of significant wave height, Journ. Geoph. Res., v 100 (C8), pp. 16149–16162.
5. Bharucha-Reid A.T. Elements of the theory of Markov Processes and their applications. MC Graw-Hill Book Company Inc., New-York, Toronto, Tokyo, 1960.
6. Belyshev A.P., Klevantsov Yu.P., Rozhkov V.A. Probabilistic analysis of sea currents. Leningrad, Gymet P.H., 1983, 264 pp. (in Russian)
7. Boukhanovsky A.V., Degtyarev A.B., Rozhkov V.A. Peculiarities of computer simulation and statistical representation of time–spatial metocean fields. LNCS #2073, Springer–Verlag, 2001, pp.463–472.
8. Boukhanovsky A.V., Mironov E.U., Rozhkov V.A. Annual rhythms and extremes of Barents sea iceness. Rev. of Russian Geographical Society, vol. 134, 3, 2002, pp. 6–16 (in Russian)
9. Boukhanovsky A.V., Krogstad H.E., Lopatoukhin L.J., Rozhkov V.A. Stochastic simulation of inhomogeneous metocean fields: Part I: Annual variability. Proc. ICCS'03, LNCS, Springer-Verlag, 2003 *(This volume)*.
10. Jardine T.P., Latham F.R. An analysis of wave heights records for the NE Atlantic. Quarterly Journal of Roy. Met. Soc., 1981, vol. 107, pp. 415–426.
11. Kallenberg O.. Random Measures. Berlin, Academie-Verlag, 1983
12. Kalnay E. et al. The NCEP/NCAR 40-Year Reanalysis Project. Bulletin of the American Meteorological Society, No. 3, March, 1996.
13. Levin B.R. Theoretical background of statistical radiophysics. Moscow, Soviet Radio, 1969
14. Loeve M. Probability theory. D. van Nostrand Company Inc., London, 1955.
15. Lopatoukhin L.J., Rozhkov V.A., Ryabinin V.E., Swail V.R., Boukhanovsky A.V., Degtyarev A.B. Estimation of extreme wave heights. JCOMM Technical Report, WMO/TD #1041, 2000.
16. Lopatoukhin L., Rozhkov V., Boukhanovsky A., Degtyarev A., Sas'kov K., Athanassoulis G., Stefanakos C., Krogstad H., The spectral wave climate in the Barents sea. Proc. OMAE 2002, paper 28397.
17. Monin A..S. An Introduction to the Theory of Climate. D. Reidel, 1986.

18. Ogorodnikov V.A., Protasov A.V. Dynamic probabilistic model of atmospheric processes and the variational methods of data assimilation. Russ. J. Numer. Anal. Math. Mod., 12, 1997, pp. 461–479.
19. Ripley B.D. Spatial statistics. NY, Chichester, Brisbane, Toronto: J. Willey & Sons, 1981.
20. Rozhkov V., Lopatoukhin L., Lavrenov I., Dymov V, Boukhanovsky A., Simulation of storm waves. Physics of Atmosphere and Ocean, 2000, 36, N5. (Translation from Russian)
21. Stefanakos Ch.N., Athanassoulis G.A., A unified methodology for the analysis, completion and simulation of nonstationary time series with missing-values, with application to wave data, Applied Ocean Research, Vol. 23/4, pp. 207–220, 2001.
22. Stefanakos Ch.N., Athanassoulis G.A., Bivariate stochastic simulation based on nonstationary time series modeling, ", 13rd International Offshore and Polar Engineering Conference, ISOPE'2003, Honolulu, Hawaii, May 25–30, 2003.
23. Tolman H. User manual and system documentation of WAVE WATCH-III. NOAA technical note. 1999.